Supplementary Information

Improving the Performance of SnS_2 Cathode with Interspace Layer Engineering Using Na^+ Insertion/Extraction Method for Aqueous Zinc Ion Batteries

Ali Molaei Aghdam *[a], Nima Mikaeili Chahartagh[b], Ehsan Delfani[b], Shahriar Namvar[c], Mahshid Ershadi[d], Farshad Boorboor Ajdari*[e,f]

[a]*Department of Chemical Engineering, Auburn University, Auburn, AL 36849, USA*

[b] *Surface Reaction and Advanced Energy Materials Laboratory, Department of Chemical Engineering, Amirkabir University of Technology (Tehran Polytechnic), PO Box 15875-4413, Tehran, Iran*

[c] *Department of Chemistry, Amirkabir University of Technology (Tehran Polytechnic), PO Box 15875-4413, Tehran, Iran*

[d]*State Key Laboratory for Mechanical Behavior of Materials, Xi'an Jiaotong University, Xi'an, 710049 P. R. China*

[e]*Department of Applied chemistry, Faculty of Chemistry, University of Kashan, Kashan, Iran*

E-mail: azm0382@auburn.edu,

farshad@xjtu.edu.cn

Materials Characterizations

On an X-ray diffractometer (Bruker D2 Phaser), the sample crystal structures were examined using copper-Kα radiation (λ = 1.54178 Å) throughout a 2θ range of 5 to 80 degrees. SEM (Philips XL 30) and TEM (Philips EM208) were used to examine the microstructure and morphology of the samples. A spectrometer (BRUKER-ALPHA) gathered Fourier transform infrared (FTIR) spectra. XPS measurements (PHI 5500) were taken to analyze the surface elemental composition and the corresponding valance states. HRTEM was performed using a field emission electron microscope (JEM-3000F (JEOL)) operating at 300 kV. EDX elemental mapping and HAADF-STEM investigations were done on a JEOL JEM-ARM200CF at 200 kV. A probe aberration corrector was installed in a STEM.

Electrochemical Measurements

The dispersion of PVDF (10 wt%) binder, super black carbon (20 wt%), and active materials (70 wt%) were performed in N-Methyl pyrrolidone. The resultant slurry was cast onto Carbon cloth to make the working electrode. The electrode was then sliced into circular slices (diameter = 11 mm) with an active mass loading of 1.75-2.1 mg cm^{-2} followed by vacuum drying at 80 °C for 10 hours. Fiber glass separator, working electrode, $ZnSO_4$ (1M) aqueous electrolyte, and zinc anode manufactured CR2032 coin cells in ambient air. Between the zinc anode and SnS_2, the separator was used to complete the AZIB. Charge-discharge cycle measurements were conducted using a Kimiastat battery test system within a voltage range from 0 to 2 V vs. Zn^{2+}/Zn. CV and electrochemical impedance spectroscopy (EIS) tests were recorded by Autolab (PGSTAT 302 N).

Materials Synthesis

Synthesis of SnS_2: SnS_2 was first synthesized by a hydrothermal method with $SnCl_2 \cdot 2H_2O$ and thiourea as the sources of tin and sulfur, respectively. In a typical synthetic process, 2 mmol $SnCl_2 \cdot 2H_2O$, 0.8 mL of HCl (mass fraction of 36-38%), and 16 mmol thiourea were dissolved into 60 mL of deionized water under vigorous magnetic stirring for 60 min to form a homogeneous solution. The solution was transferred into a 100 mL Teflon-lined stainless-steel autoclave followed by hydrothermal treatment at 145 °C for 24 h. After the autoclave was cooled to room temperature naturally, the obtained primary product, i.e., SnS_2, was centrifuged and washed several times by deionized water and absolute ethyl alcohol and finally dried at 60 °C for 12 h in the air environment.

Synthesis of SnS_2-HIL: To increase the interspace layer of SnS_2, we used sodium ion insertion/extraction method. The coin-type cell was assembled with a cathode, fiber glass as a separator, and zinc foil as an anode. For the sodium source, we used 1M sodium sulfate electrolyte. Insertion/ extraction Na ion was conducted under constant current protocol using are battery tester within a voltage range of 0–2 V vs. Zn/Zn^{2+}.

Zn-ions diffusion coefficient calculation based on the GITT measurement:

The kinetics of Zn^{2+} intercalation during the charge/discharge reaction of SnS_2-HIL cathode material in depth was investigated using the galvanostatic intermittent titration technique (GITT). The diffusion coefficient of Zn^{2+} (D_{Zn}) was calculated using the following equation:

$$D_{Zn} = \frac{4}{\pi\tau}\left(\frac{mV_m}{MA}\right)^2\left(\frac{\Delta E_s}{\Delta E_\tau}\right)^2$$

Where τ, M, m, V_m, A severally represented the relaxation time, the molar mass of active material, the mass of active material, the molar volume, and the contact area between electrode and electrolyte, while ΔEs and ΔEτ represented the values of pulse voltage change and voltage change of constant-current charge/discharge, respectively.

Zn-ions concentration calculation:

Firstly, the unit cell volume of SnS_2-HIL was calculated by"*a* (3.826Å) × *b* (3.826Å) × *c* (3.826Å) × sin45° = **39.601**× 10^{-24} cm^3", thereby 1 cm^3 contains 1/39.601 × 10^{-24} = 2.25 × 10^{22} unit cells. Since each SnS_2-HIL unit cell contains two molecules, and each molecule contains 0.9 Zn-ions, 1 cm^3 contains 2.25 × 10^{22}/6.02 × 10^{23} × 8 × 0.9 = 5.15 × 10^{-3} mol Zn-ions. Therefore, the Zn-ions concentration in the electrode is approximately 5.15 × 10^{-3} mol cm^{-3}[1].

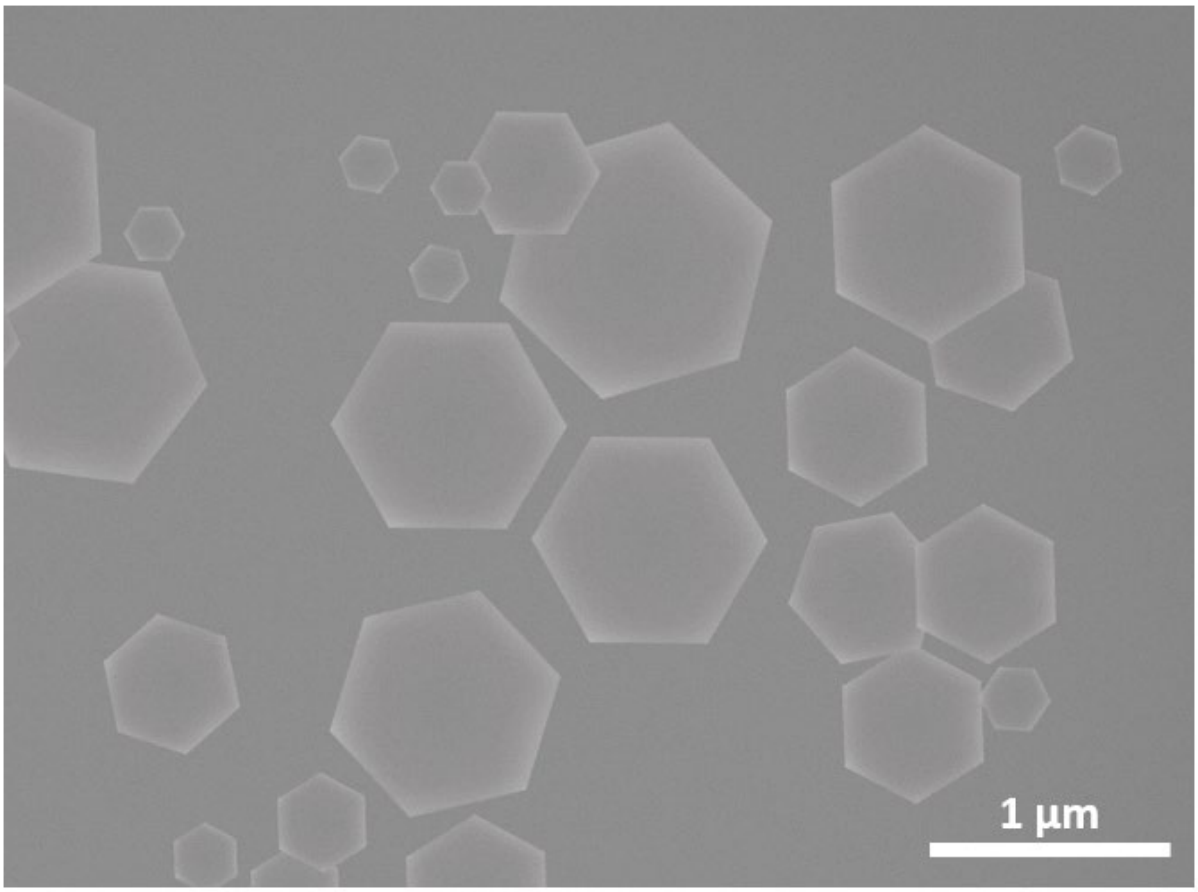

Figure S1. SEM image of SnS_2

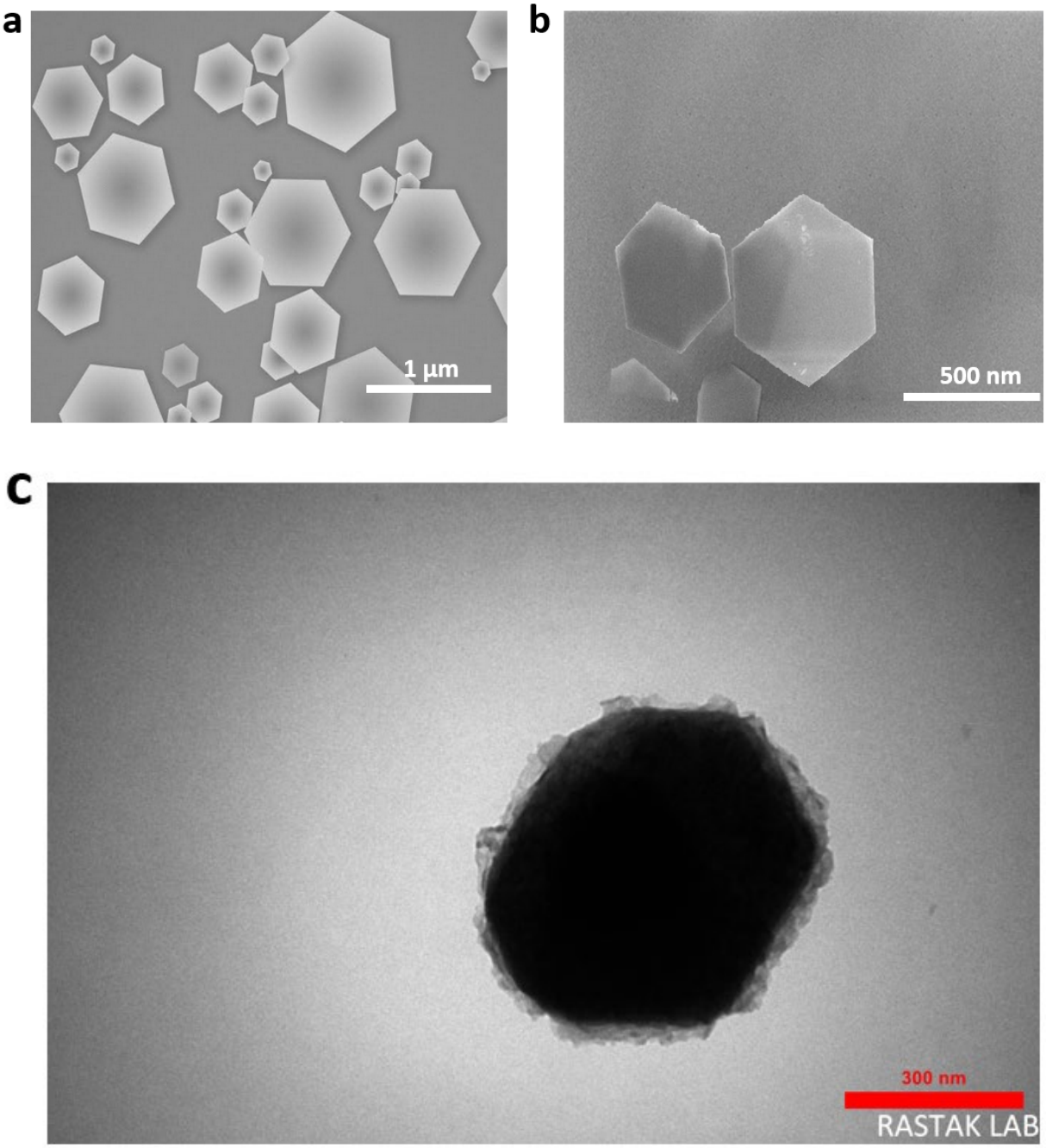

Figure S2. a,b) SEM image of SnS_2 after insertion/extraction Na^+. c) TEM image of SnS_2 after insertion/extraction Na^+.

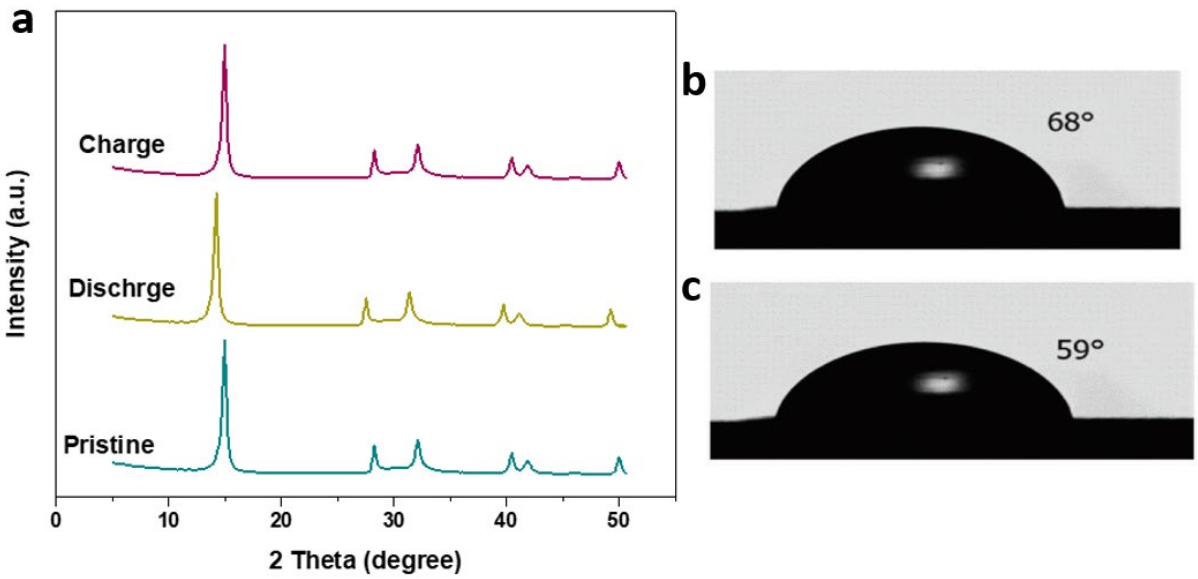

Figure S3. a) XRD for pristine SnS_2 and SnS_2 cathodes after insertion/extraction Na^+. Water contact angles of b) pristine SnS_2 and c) after insertion/extraction Na^+.

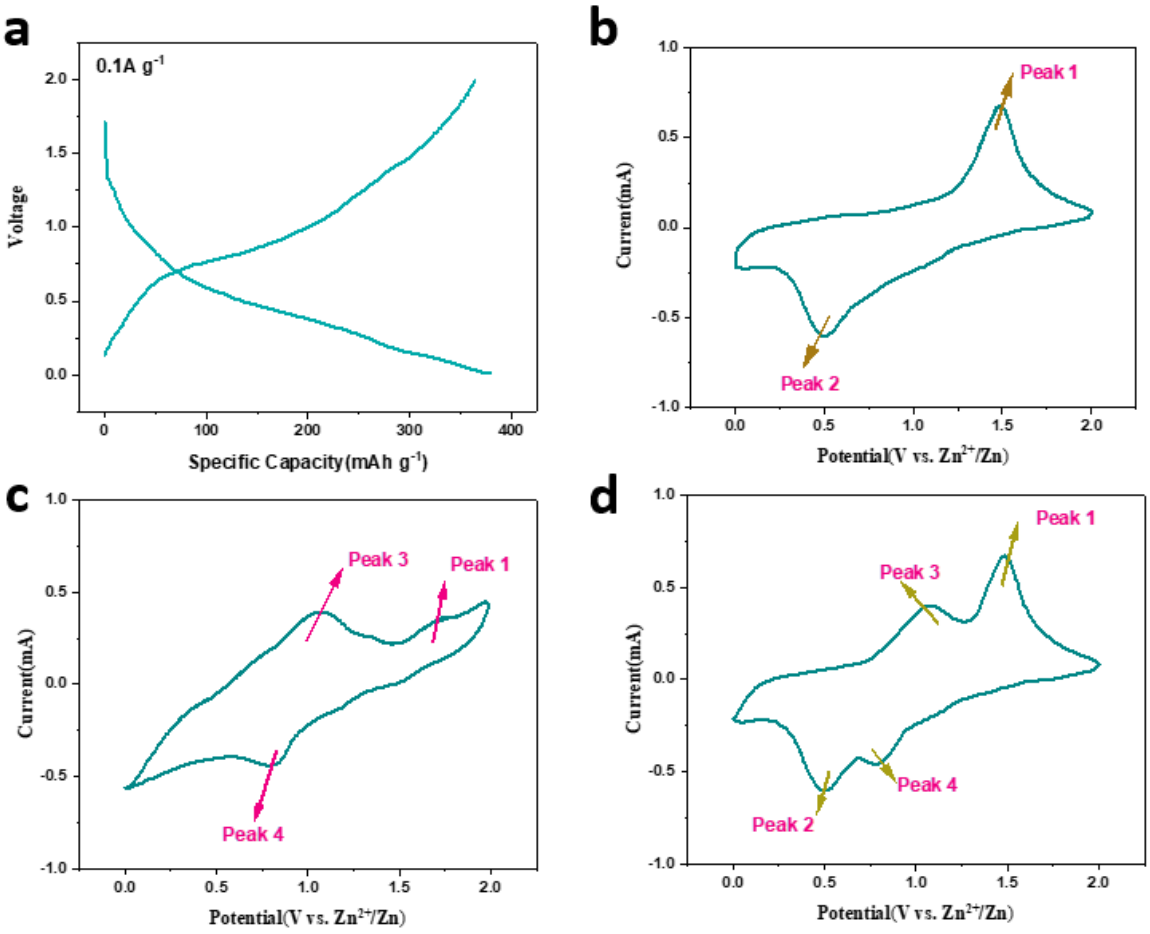

Figure S4. a)charge/discharge curves at 0.1 A g^{-1} over the voltage range of 0-2 V of the SnS_2 cathode for Na^+ insertion/extraction in 1M Na_2SO_4. CV curves of SnS_2 cathodes at a scan rate of 0.3 mV s^{-1} in b) 1M $ZnSO_4$, c) 1M Na_2SO_4, and d) 1M Na_2SO_4 + 1M $ZnSO_4$

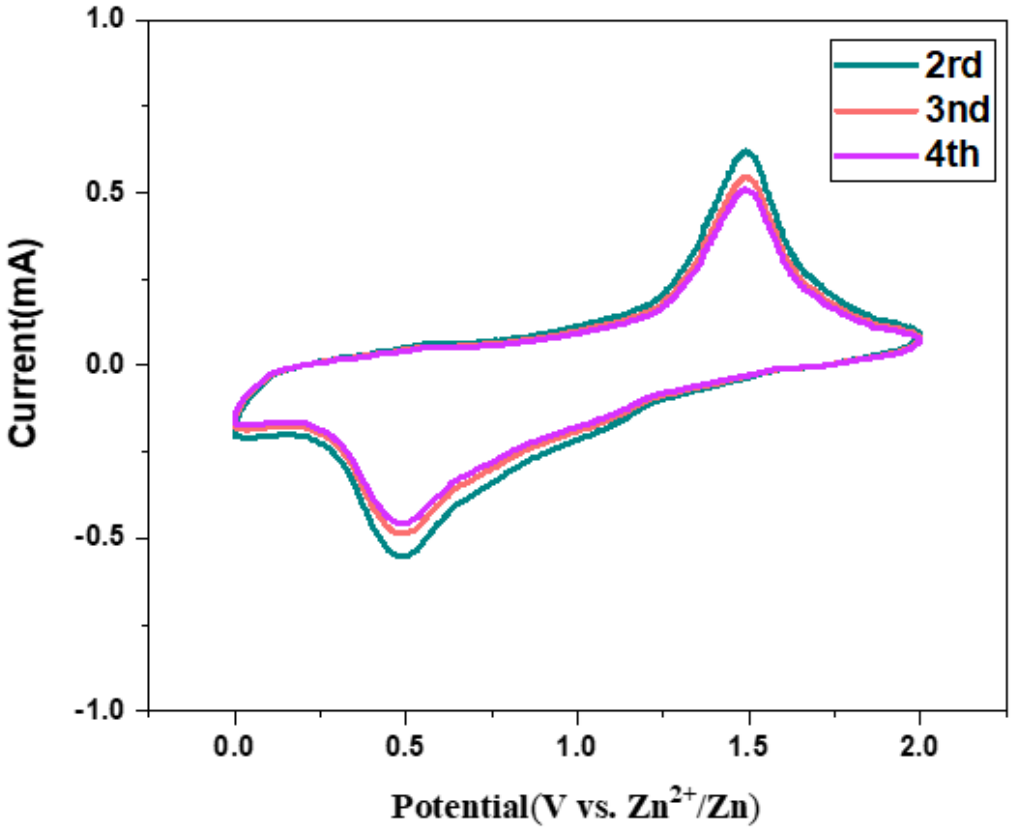

Figure S5. CV curves of SnS_2 cathodes at a scan rate of 0.3 mV s^{-1}.

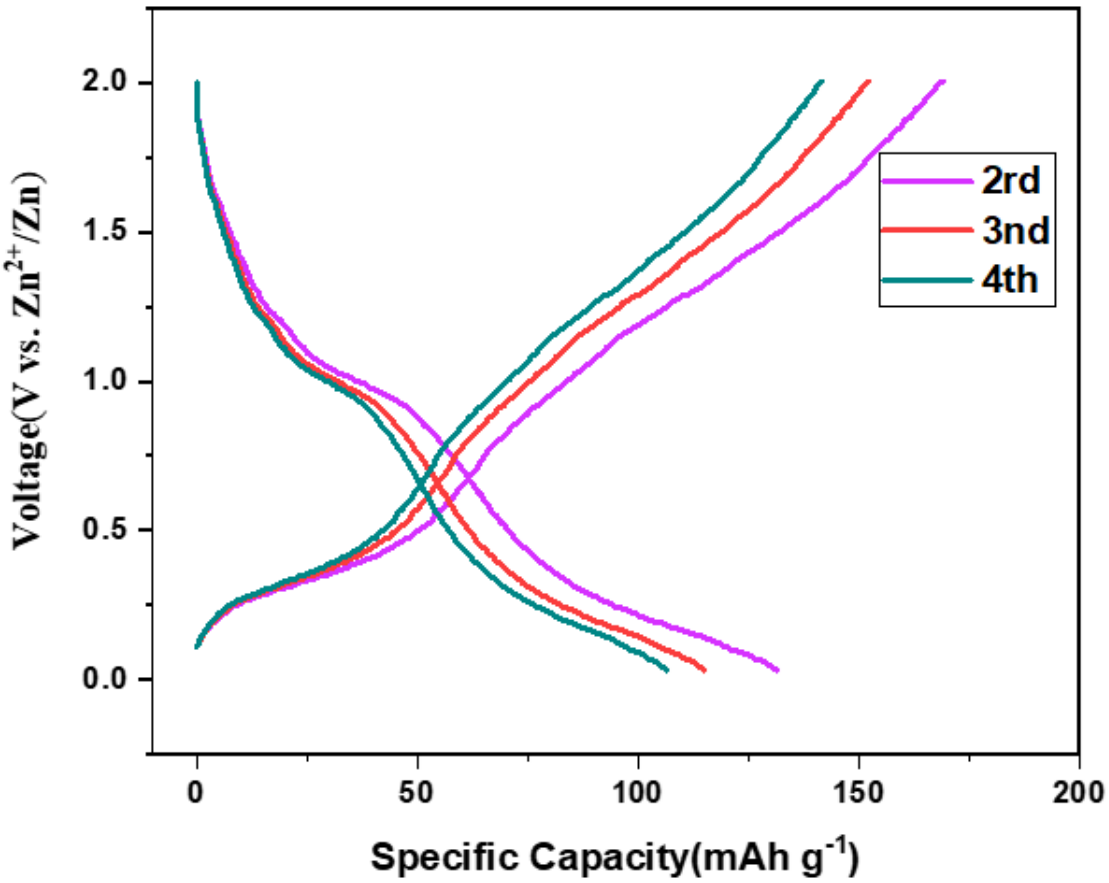

Figure S6. charge/discharge curves at 0.1 A g^{-1} over the voltage range of 0-2 V of the SnS_2 cathode.

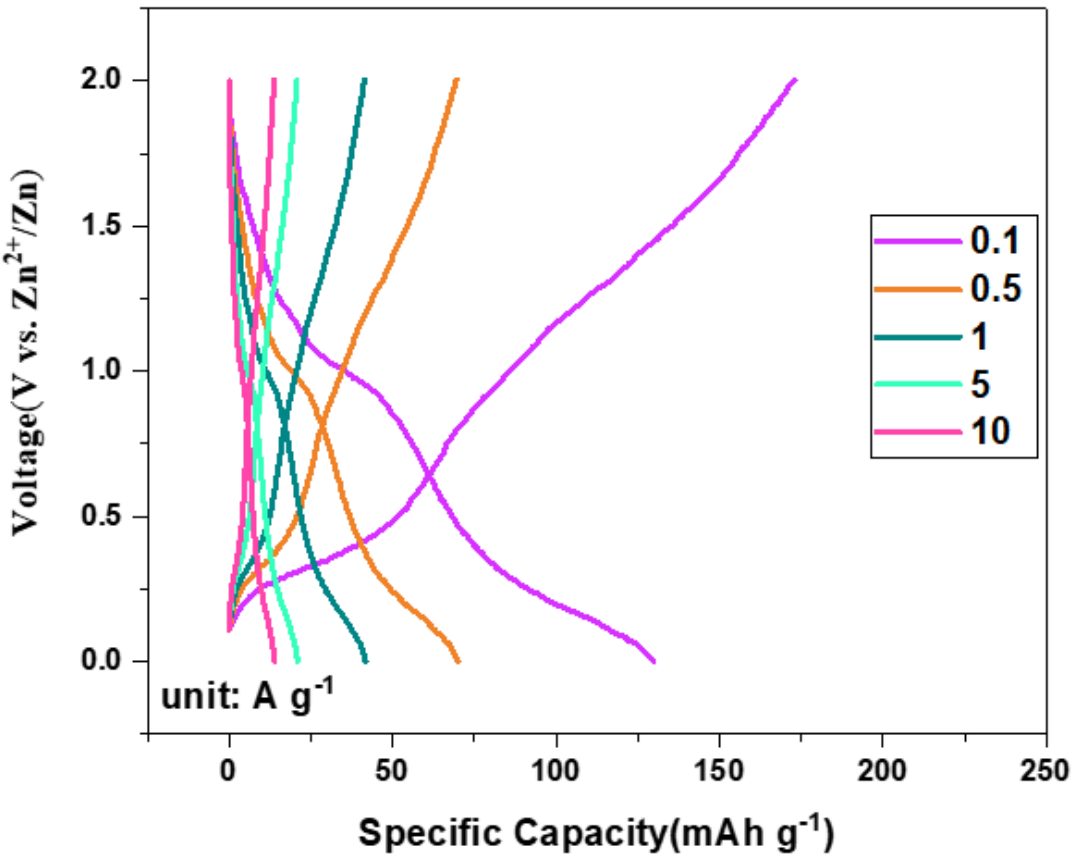

Figure S7. Typical galvanostatic charge and discharge profiles of SnS_2 cathode for different current densities.

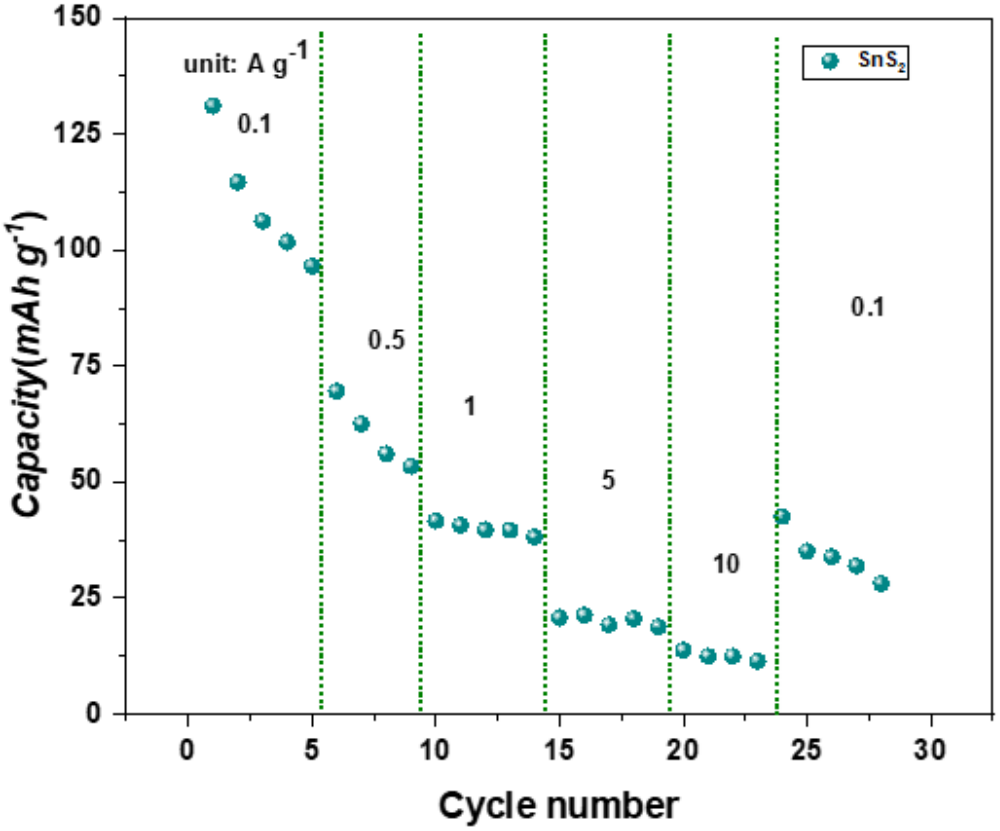

Figure S8. Rate capability at 0.1-10 A g^{-1} of SnS_2 cathode

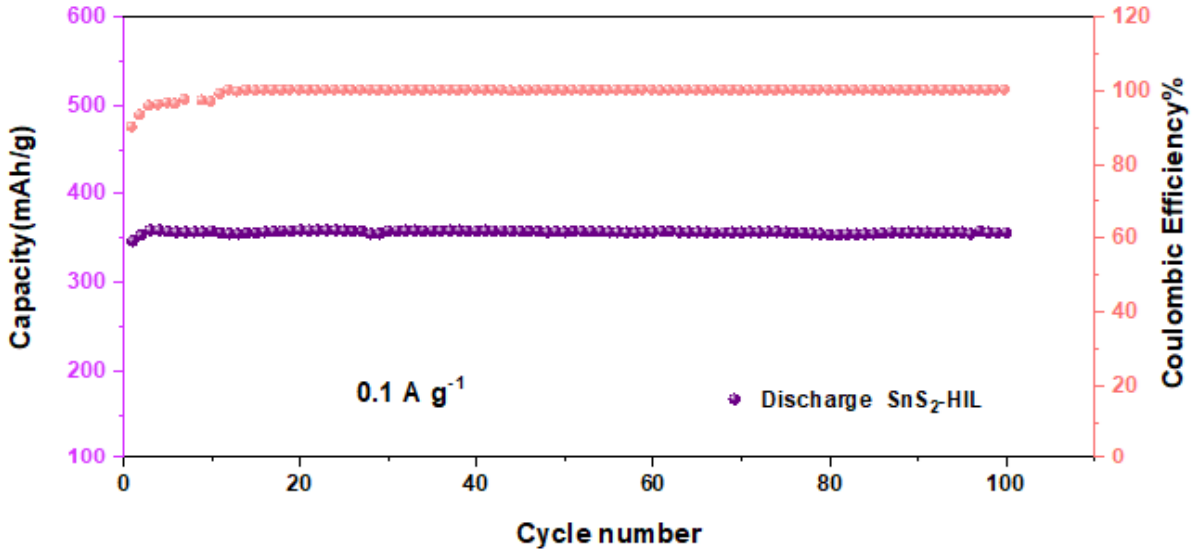

Figure S9 cycling performance at 0. 1 A g^{-1} of the SnS_2-HILcathode.

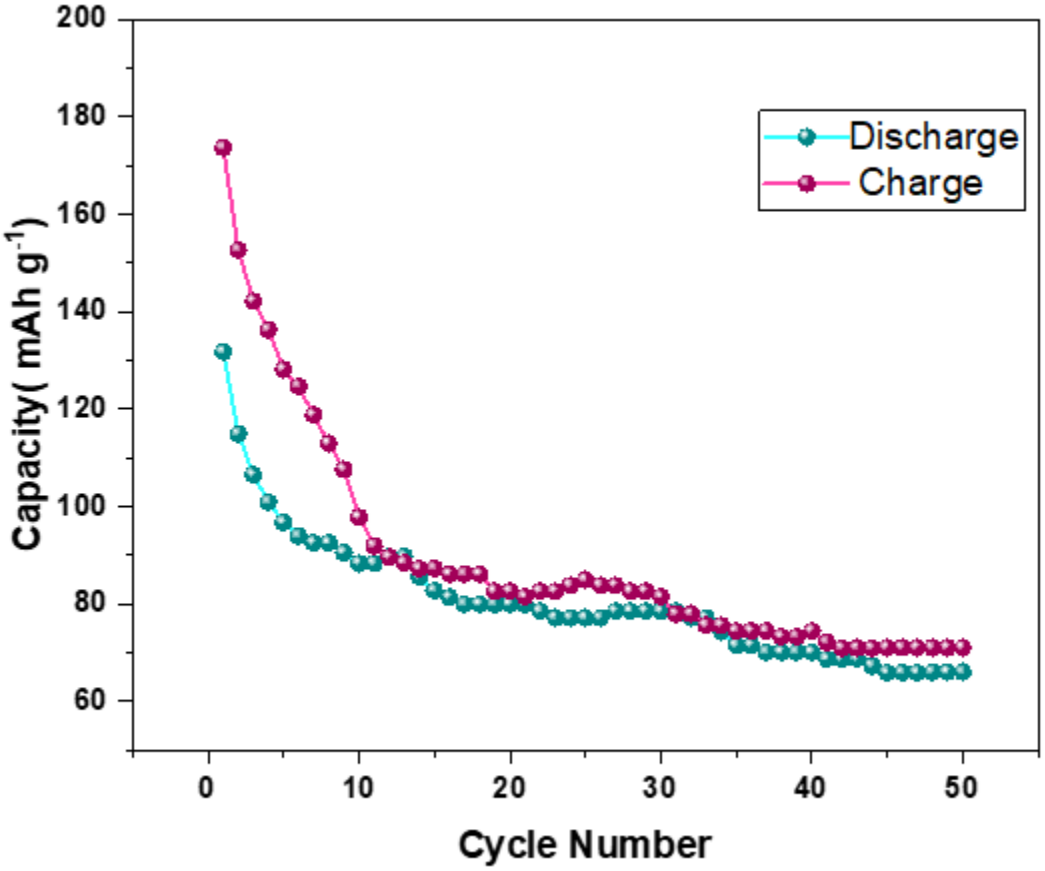

Figure S10 cycling performance at 0.1 A g^{-1} of the pristine SnS_2 cathode.

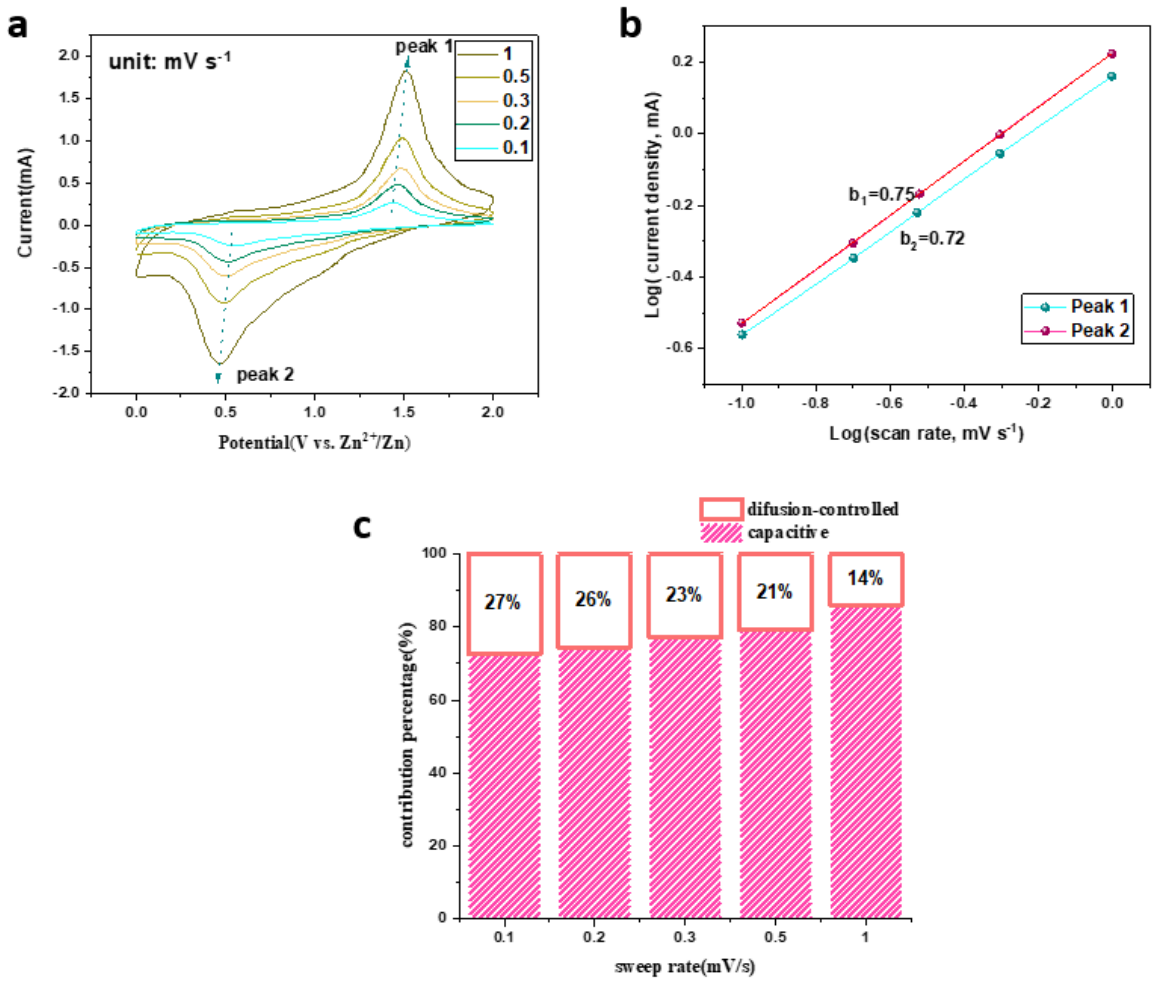

Figure S11. a) CV curves of SnS_2 cathode at various scan rates. b) Plots of log i versus log v at specific peak currents. c) The percentage of capacitive contributions for SnS_2 cathode at various sweep rates.

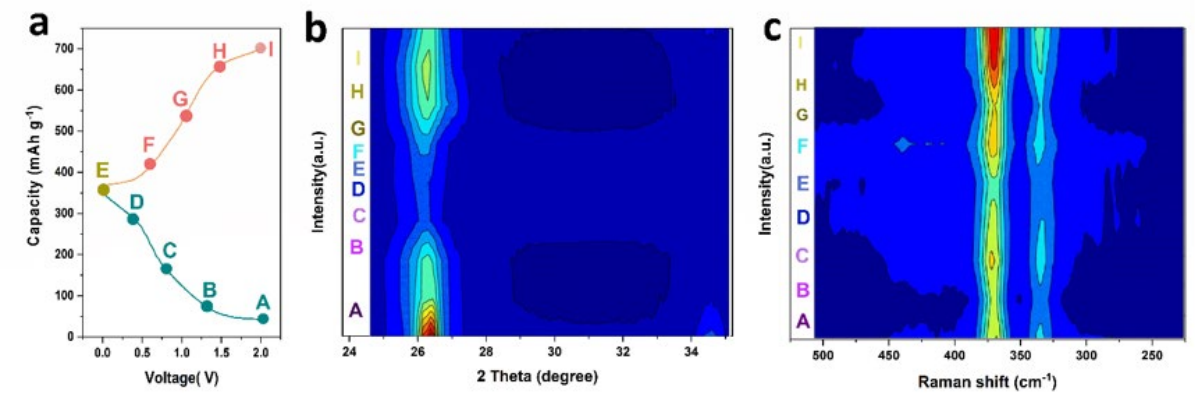

Figure S12 a) initial discharge/charge curve at 0.1 A g^{-1}, the marked states are chosen for ex-situ tests; b) ex-situ XRD patterns; c) ex-situ Raman spectra

Table S1. Summary of the electrochemical properties of transition-metal sulfides and selenides cathodes

Cathode materials	Electrolyte	Voltage	Capacity [mAh g^{-1}]	Cycle stability	Ref
SnS_2-HIL	1m $ZnSO_4$	0-2 V	359 mAh g^{-1}	83.7 after 1000 cycles at 5 A g^{-1}	In this work
MoS_2/PANI	3 m $Zn(CF_3SO_3)_2$	0.2–1.3 V	106.5 at 1.0 A g^{-1}	86% after 1000 cycles at 1.0 A g^{-1}	2
MoS_2@CF	3 m $Zn(CF_3SO_3)_2$	0.2–1.3 V	182 at 0.1 A g^{-1}	94% over 1500 cycles at 2 A g^{-1}	3
MoS_2-nH_2O	3 m $Zn(CF_3SO_3)_2$	0.2–1.25 V	165 at 0.1 A g^{-1}	88% over 800 cycles at 1 A g^{-1}	4
1T MoS_2	3 m $Zn(CF3SO3)_2$	0.25–1.25 V	165 at 0.1 A g^{-1}	98.1% over 400 cycles at 1 A g^{-1}	5
200-MoS2	3 m $Zn(CF_3SO3)_2$	0.25–1.3 V	148 at 0.5 A g^{-1}	100% after 500 cycles at 2 A g^{-1}	6
Vertical 1T-MoS_2	3 m $Zn(CF_3SO_3)_2$	0.25–1.25 V	198 at 0.1 A g^{-1}	87.8% after 2000 cycles at 1 A g^{-1}	7
1T VS_2	1 m $ZnSO_4$	0.4–1.0 V	190 at 0.01 A g^{-1}	98% after 200 cycles at 0.5 A g^{-1}	8
VS_2@SS	1 m $ZnSO_4$	0.4–1.0 V	190 at 0.05 A g^{-1}	80% after 2000 cycles at 2 A g^{-1}	9
1T WS_2	1 m $ZnSO_4$	0.1–1.5 V	233.26 at 0.05 A g^{-1}	/	10
$TiSe_2$	2 m $ZnSO_4$	0.05–0.6 V	128 at 0.2 A g^{-1}	70% after 300 cycles at 1.0 A g^{-1}	11
VSe_{2-x}-SS	3 m $Zn(CF_3SO_3)_2$	0.4–1.6 V	265.2 at 0.2 A g^{-1}	87.8% over 1800 cycles at 4 A g^{-1}	12
D-MoS_2-O	3 m $Zn(CF_3SO_3)_2$	0.2–1.25 V	261 at 0.1 A g^{-1}	90.5% after 1000 cycles at 1 A g^{-1}	13
Sn vacancy $Co_3Sn_{1.8}S_2$	1 m $Zn(TFSI)_2$	0.01–2.3 V	346 at 0.2 A g^{-1}	83.3% over 2400 cycles at 1 A g^{-1}	14
N-doped 1T MoS_2	3 m $Zn(CF_3SO_3)_2$	0.2–1.3 V	149.6 at 0.1 A g^{-1}	89.1% after 1000 cycles at 3 A g^{-1}	15
VS_2@N-C	3 m $Zn(CF_3SO_3)_2$	0.2–1.8 V	203 at 0.05 A g^{-1}	97% after 600 cycles at 1 A g^{-1}	16
Co-doped $Ni3Se_2$	1 m KOH and 0.25 m ZnO	1.4–1.9 V	179.34 at 1 A g^{-1}	85.9% after 1000 cycles at 1 A g^{-1}	17
MoS_2/Graphene	3 m $Zn(CF_3SO_3)_2$	0.2–1.5 V	283.9 at 0.1 A g^{-1}	88.6% after 1800 cycles at 1 A g^{-1}	18
MoS_2@CNTs	3 m $Zn(CF_3SO_3)_2$	0.3–1.2 V	161.5 at 0.1 A g^{-1}	80.1% after 500 cycles at 1 A g^{-1}	19
rGO-VS_2	3 m $Zn(CF_3SO_3)_2$	0.4–1.7 V	238 at 0.1 A g^{-1}	93% after 1000 cycles at 5.0 A g^{-1}	20
rGO-VSe_2	2 m $ZnSO_4$	0.2–1.4 V	221.5 at 0.5 A g^{-1}	91.6% after 150 cycles at 0.5 A g^{-1}	21
VS_4@rGO	1 m $Zn(CF_3SO_3)_2$	0–1.8 V	450 at 0.5 A g^{-1}	82% after 3500 cycles at 10 A g^{-1}	22
MoS3/MWCNTs	2 m $ZnSO_4$	0.01–2 V	368 at 0.5 A g-1	85.6% after 100 cycles at 0.5 A g^{-1}	23
MnS/RGO	2 m $ZnSO_4$ and 0.1 m $MnSO_4$	0.8–1.9 V	289 at 0.1 A g^{-1}	70.8% after 1000 cycles at 1 A g^{-1}	24
VS2@VOOH	3 m $Zn(CF_3SO3)_2$	0.4–1.0 V	165 at 0.1 A g^{-1}	86% after 200 cycles at 1.0 A g^{-1} [123]	25
VS2/VOx	25 m $ZnCl_2$	0.1–1.8 V	260 at 0.1 A g^{-1}	75% after 3000 cycles at 1.0 A g^{-1} [142]	26

References

1. Liu, Y. *et al.* Approaching the Downsizing Limit of Maricite NaFePO4 toward High-Performance Cathode for Sodium-Ion Batteries. *Adv. Funct. Mater.* **28**, (2018).
2. Huang, M. *et al.* Tuning the kinetics of zinc ion in MoS2 by polyaniline intercalation. *Electrochim. Acta* **388**, (2021).
3. Liu, H. *et al.* Boosting zinc-ion intercalation in hydrated MoS2 nanosheets toward substantially improved performance. *Energy Storage Mater.* **35**, 731–738 (2021).
4. Zhang, Z. *et al.* Crystal water assisting MoS2 nanoflowers for reversible zinc storage. *J. Alloys Compd.* (2021) doi:10.1016/j.jallcom.2021.159599.
5. Liu, J. *et al.* Boosting aqueous zinc-ion storage in MoS2 via controllable phase. *Chem. Eng. J.* **389**, (2020).
6. Cai, C. *et al.* A nano interlayer spacing and rich defect 1T-MoS 2 as cathode for superior performance aqueous zinc-ion batteries . *Nanoscale Adv.* **3**, 3780–3787 (2021).
7. Liu, J. *et al.* Vertically aligned 1 T phase MoS2 nanosheet array for high-performance rechargeable aqueous Zn-ion batteries. *Chem. Eng. J.* **428**, (2022).
8. He, P. *et al.* Layered VS2 nanosheet-based aqueous Zn ion battery cathode. *Adv. Energy Mater.* **7**, 1601920 (2017).
9. Jiao, T. *et al.* Binder-free hierarchical VS2 electrodes for high-performance aqueous Zn ion batteries towards commercial level mass loading. *J. Mater. Chem. A* **7**, 16330–16338 (2019).
10. Tang, B. *et al.* Investigation of zinc storage capacity of WS2 nanosheets for rechargeable aqueous Zn-ion batteries. *J. Alloys Compd.* **894**, (2022).
11. Wen, L. *et al.* A novel TiSe2 (de)intercalation type anode for aqueous zinc-based energy storage. *Nano Energy* vol. 93 (2022).
12. Bai, Y. *et al.* Selenium Defect Boosted Electrochemical Performance of Binder-Free VSe2Nanosheets for Aqueous Zinc-Ion Batteries. *ACS Appl. Mater. Interfaces* **13**, 23230–23238 (2021).
13. Li, S. *et al.* Molecular Engineering on MoS2 Enables Large Interlayers and Unlocked Basal Planes for High-Performance Aqueous Zn-Ion Storage. *Angew. Chemie - Int. Ed.* **60**, 20286–20293 (2021).
14. Zhao, Y. *et al.* Vacancy Modulating Co3Sn2S2 Topological Semimetal for Aqueous Zinc-Ion Batteries. *Angew. Chemie - Int. Ed.* **61**, (2022).
15. Sheng, Z. *et al.* Nitrogen-Doped Metallic MoS2Derived from a Metal-Organic Framework for Aqueous Rechargeable Zinc-Ion Batteries. *ACS Appl. Mater. Interfaces* **13**, 34495–34506 (2021).
16. Liu, J., Peng, W., Li, Y., Zhang, F. & Fan, X. A VS2@N-doped carbon hybrid with strong interfacial

interaction for high-performance rechargeable aqueous Zn-ion batteries. *J. Mater. Chem. C* **9**, 6308–6315 (2021).

17. Amaranatha Reddy, D. *et al.* Facile synthesis of cauliflower-like cobalt-doped Ni3Se2 nanostructures as high-performance cathode materials for aqueous zinc-ion batteries. *Int. J. Hydrogen Energy* **45**, 7741–7750 (2020).

18. Li, S. *et al.* Sandwich-Like Heterostructures of MoS2/Graphene with Enlarged Interlayer Spacing and Enhanced Hydrophilicity as High-Performance Cathodes for Aqueous Zinc-Ion Batteries. *Adv. Mater.* **33**, (2021).

19. Huang, M. *et al.* Hierarchical MoS2@CNTs Hybrid as a Long-Life and High-Rate Cathode for Aqueous Rechargeable Zn-Ion Batteries. *ChemElectroChem* **7**, 4218–4223 (2020).

20. Chen, T. *et al.* VS2 nanosheets vertically grown on graphene as high-performance cathodes for aqueous zinc-ion batteries. *J. Power Sources* **477**, (2020).

21. Narayanasamy, M. *et al.* Nanohybrid engineering of the vertically confined marigold structure of rGO-VSe2 as an advanced cathode material for aqueous zinc-ion battery. *J. Alloys Compd.* **882**, (2021).

22. Chen, K. *et al.* Robust VS4@rGO nanocomposite as a high-capacity and long-life cathode material for aqueous zinc-ion batteries. *Nanoscale* **13**, 12370–12378 (2021).

23. Liu, Y. *et al.* Performance and application of carbon composite MoS3 as cathode materials for aqueous zinc-ion batteries. *J. Alloys Compd.* **893**, (2022).

24. Ma, S. C. *et al.* In situ preparation of manganese sulfide on reduced graphene oxide sheets as cathode for rechargeable aqueous zinc-ion battery. *J. Solid State Chem.* **299**, (2021).

25. Pu, X. *et al.* Rose-like vanadium disulfide coated by hydrophilic hydroxyvanadium oxide with improved electrochemical performance as cathode material for aqueous zinc-ion batteries. *J. Power Sources* **437**, (2019).

26. Yu, D. *et al.* Boosting Zn2+ and NH4+ Storage in Aqueous Media via In-Situ Electrochemical Induced VS2/VOx Heterostructures. *Adv. Funct. Mater.* **31**, (2021).